Eur. Phys. J. C 18, 41–55 (2000)
Digital Object Identifier (DOI) 10.1007/s100520000504

THE EUROPEAN PHYSICAL JOURNAL C

A detailed description of the analysis of the decay of neutral kaons to $\pi^+\pi^-$ in the CPLEAR experiment

The CPLEAR Collaboration

A. Apostolakis[1], E. Aslanides[11], G. Backenstoss[2], P. Bargassa[13], O. Behnke[17], A. Benelli[2], V. Bertin[11], F. Blanc[7,13], P. Bloch[4], P. Carlson[15], M. Carroll[9], E. Cawley[9], M.B. Chertok[3], M. Danielsson[15], M. Dejardin[14], J. Derre[14], A. Ealet[11], C. Eleftheriadis[16], W. Fetscher[17], M. Fidecaro[4], A. Filipčič[10], D. Francis[3], J. Fry[9], E. Gabathuler[9], R. Gamet[9], H.-J. Gerber[17], A. Go[4], A. Haselden[9], P.J. Hayman[9], F. Henry-Couannier[11], R.W. Hollander[6], K. Jon-And[15], P.-R. Kettle[13], P. Kokkas[2], R. Kreuger[6], R. Le Gac[11], F. Leimgruber[2], I. Mandić[10], N. Manthos[8], G. Marel[14], M. Mikuž[10], J. Miller[3], F. Montanet[11], A. Muller[14] T. Nakada[13], B. Pagels[17], I. Papadopoulos[16], P. Pavlopoulos[2], G. Polivka[2], R. Rickenbach[2], B.L. Roberts[3], T. Ruf[4], L. Sakeliou[1], M. Schäfer[17], L.A. Schaller[7], T. Schietinger[2], A. Schopper[4], L. Tauscher[2], C. Thibault[12], F. Touchard[11], C. Touramanis[9], C.W.E. Van Eijk[6], S. Vlachos[2], P. Weber[17], O. Wigger[13], M. Wolter[17], C. Yeche[14], D. Zavrtanik[10], D. Zimmerman[3]

[1] University of Athens, 10680 Athens, Greece
[2] University of Basle, 4056 Basle, Switzerland
[3] Boston University, Boston, MA 02215, USA
[4] CERN, Geneva, 1211 Genève, Switzerland
[5] LIP and University of Coimbra, 3000 Coimbra, Portugal
[6] Delft University of Technology, 2629 JB Delft, Netherlands
[7] University of Fribourg, 1700 Fribourg, Switzerland
[8] University of Ioannina, 45110 Ioannina, Greece
[9] University of Liverpool, Liverpool L69 7ZE, UK
[10] J. Stefan Inst. and Phys. Dept., University of Ljubljana, 61111 Ljubljana, Slovenia
[11] CPPM, IN2P3-CNRS et Université d'Aix-Marseille II, 13288 Marseille, France
[12] CSNSM, IN2P3-CNRS, 91405 Orsay, France
[13] Paul Scherrer Institut (PSI), 5232 Villigen-PSI, Switzerland
[14] CEA, DSM/DAPNIA, CE-Saclay, 91191 Gif-sur-Yvette France
[15] Royal Institute of Technology, 10405 Stockholm, Sweden
[16] University of Thessaloniki, 54006 Thessaloniki, Greece
[17] ETH-IPP Zürich, 8093 Zürich, Switzerland

Received: 8 May 2000 / Published online: 13 November 2000 – © Springer-Verlag 2000

Abstract. A detailed description is given of the analysis of neutral kaons decaying to $\pi^+\pi^-$, based on the complete set of data collected with the CPLEAR experiment. Using a novel approach involving initially strangeness-tagged K^0 and $\overline{K}^0$, the time-dependent decay-rate asymmetry has been measured. This asymmetry, resulting from the interference between the K_S and K_L decay amplitudes, has enabled both the magnitude and phase of the CP-violation parameter, η_{+-}, to be measured, with a precision comparable to that of the current world-average values.

1 Introduction

The CPLEAR experiment, at the Low Energy Antiproton Ring (LEAR) at CERN, has developed a novel approach to the study of CP, T and CPT symmetries in the decay of neutral kaons. In this approach, the strangeness of the neutral kaons at production is tagged and then decay-rate asymmetries are measured for decays to a variety of final states. From these asymmetries, parameters describing the violation of CP, T and CPT are determined with small systematic uncertainties [1].

In this paper we give a detailed description of the analysis of neutral kaons decaying to $\pi^+\pi^-$, based on the complete set of data collected by CPLEAR between 1992 and 1996. From these data, both the magnitude $|\eta_{+-}|$ and phase ϕ_{+-} of the parameter η_{+-}, describing CP violation in this channel, are determined. A letter giving these results for η_{+-} has already been published [2]. The experiment has reached a precision comparable to that obtained from compilations [3,4] of results of previous experiments, with ϕ_{+-} values from [5–9,11] and $|\eta_{+-}|$ values from [3,5,10,11]. The compilation fits include results

on other neutral-kaon experimental information, like K_S-K_L mass difference, and K_S and K_L mean lifetimes and branching ratios [3].

A precise measurement of the parameter η_{+-} is of interest in its own right, but, in addition, a comparison of its phase, ϕ_{+-}, with the superweak phase, ϕ_{sw}, in combination with the values of other parameters measured by CPLEAR, provides a stringent indirect test of CPT invariance [12]. Moreover, the CPLEAR $\pi^+\pi^-$ data, in conjuction with CPLEAR semileptonic data and results from other experiments at later decay times, may be used to place limits on parameters describing the possible evolution of pure states into mixed states, sensitive to physics at ultra-high energies [14–16]. Such limits were calculated in [14] using a subset of the total CPLEAR data [11,13] and data from [5].

In Sect. 2, the phenomenology of neutral-kaon decays to $\pi^+\pi^-$ is described. In Sect. 3 we describe the experimental method used to extract the parameter η_{+-}. The CPLEAR experiment is presented in Sect. 4 followed by the event selection and comparison with simulated data in Sect. 5. Corrections applied to the data are detailed in Sect. 6 and the final results are reported in Sect. 7. A summary of the results and their significance is given in Sect. 8.

2 Phenomenology of neutral-kaon decays to $\pi^+\pi^-$

The strong and electromagnetic interactions conserve strangeness and have well defined strangeness eigenstates K^0 and $\overline{K}^0$. The weak interaction does not conserve strangeness and causes the two strangeness eigenstates to mix ($|\Delta(S)| = 2$ processes) and also causes neutral kaons to decay to non-strange final states ($|\Delta(S)| = 1$ processes). The time evolution of the K^0-$\overline{K}^0$ state, including its decay products, is described by the Schrödinger equation with a total Hamiltonian $H_{st} + H_{em} + H_{wk}$. The weak interaction (H_{wk}) is much weaker than either the strong (H_{st}) or electromagnetic (H_{em}) interaction. Therefore a perturbation calculation may be used to eliminate the explicit appearance of the decay products in the time dependence of the neutral-kaon system, which leads to

$$|\psi(t)\rangle = a(t)\ \left|K^0\right\rangle + b(t)\ \left|\overline{K}^0\right\rangle ,$$

satisfying

$$\mathrm{i}\frac{\partial}{\partial t}\begin{pmatrix} a(t) \\ b(t) \end{pmatrix} \ = \ \Lambda \begin{pmatrix} a(t) \\ b(t) \end{pmatrix} , \qquad (1)$$

where Λ is a complex, two-by-two matrix and is expressed in terms of two hermitian matrices M (the mass matrix), and Γ (the decay matrix), as $\Lambda = M - \frac{\mathrm{i}}{2}\Gamma$. The diagonal elements of these matrices, $M_{11}, M_{22}, \Gamma_{11}$ and Γ_{22} signify the masses and decay widths of K^0 and $\overline{K}^0$ respectively. The eigenvalues of (1) are

$$\lambda_{S,L} \ = \ m_{S,L} - \tfrac{\mathrm{i}}{2}\Gamma_{S,L}$$

and the corresponding eigenstates are $|K_S\rangle$ and $|K_L\rangle$, which have definite masses and decay widths, $m_{S,L}$ and $\Gamma_{S,L}$. Assuming any violation of T or CPT invariance to be small, these are given by:

$$|K_S\rangle = \frac{1}{\sqrt{2}}\Big[(1+\varepsilon+\delta)\ \left|K^0\right\rangle + (1-\varepsilon-\delta)\ \left|\overline{K}^0\right\rangle\Big] , \quad (2a)$$

$$|K_L\rangle = \frac{1}{\sqrt{2}}\Big[(1+\varepsilon-\delta)\ \left|K^0\right\rangle - (1-\varepsilon+\delta)\ \left|\overline{K}^0\right\rangle\Big] , \quad (2b)$$

where the parameters ε and δ describe T and CP violation with CPT invariance, and CPT and CP violation with T invariance, respectively. These are given by:

$$\varepsilon = \frac{\Lambda_{21} - \Lambda_{12}}{2\Delta\lambda} \quad \text{and} \quad \delta = \frac{\Lambda_{22} - \Lambda_{11}}{2\Delta\lambda} ,$$

with $\Delta\lambda = \lambda_L - \lambda_S = \Delta m + \frac{\mathrm{i}}{2}\Delta\Gamma$; $\Delta m = m_L - m_S$; $\Delta\Gamma = \Gamma_S - \Gamma_L$. The off-diagonal elements of Λ, $|M_{12}|\mathrm{e}^{\mathrm{i}\phi_M} - \frac{\mathrm{i}}{2}|\Gamma_{12}|\mathrm{e}^{\mathrm{i}\phi_\Gamma}$ and $|M_{12}|\mathrm{e}^{-\mathrm{i}\phi_M} - \frac{\mathrm{i}}{2}|\Gamma_{12}|\mathrm{e}^{-\mathrm{i}\phi_\Gamma}$, are related to Δm and $\Delta\Gamma$ as $2|M_{12}| = \Delta m$ and $2|\Gamma_{12}| = \Delta\Gamma$. The arbitrariness of the phases of the K^0 and $\overline{K}^0$ states allows us to choose $\phi_\Gamma = 0$ or close to 0.

For initially pure K^0 and $\overline{K}^0$ states, the solutions of (1) are:

$$\begin{aligned} \left|K^0(t)\right\rangle &= [f_+(t) + 2\delta f_-(t)]\ \left|K^0\right\rangle + (1-2\varepsilon) f_-(t)\ \left|\overline{K}^0\right\rangle \\ &= \frac{1}{\sqrt{2}}[(1-\varepsilon+\delta)\mathrm{e}^{-\mathrm{i}\lambda_S t}\ |K_S\rangle + (1-\varepsilon-\delta)\mathrm{e}^{-\mathrm{i}\lambda_L t} \\ &\quad \times |K_L\rangle] , \qquad (3a) \\ \left|\overline{K}^0(t)\right\rangle &= [f_+(t) - 2\delta f_-(t)]\ \left|\overline{K}^0\right\rangle + (1+2\varepsilon) f_-(t)\ \left|K^0\right\rangle \\ &= \frac{1}{\sqrt{2}}[(1+\varepsilon-\delta)\mathrm{e}^{-\mathrm{i}\lambda_S t}\ |K_S\rangle - (1+\varepsilon+\delta)\mathrm{e}^{-\mathrm{i}\lambda_L t} \\ &\quad \times |K_L\rangle] , \qquad (3b) \end{aligned}$$

with the time-dependent functions given by $f_\pm(t) = \frac{1}{2}(\mathrm{e}^{-\mathrm{i}\lambda_S t} \pm \mathrm{e}^{-\mathrm{i}\lambda_L t})$. If the amplitude for the decay of a K_S or a K_L to a final state f is defined as

$$A_{fS} = \langle f|\ H_{wk}\ |K_S\rangle\ , \quad A_{fL} = \langle f|\ H_{wk}\ |K_L\rangle\ , \quad (4)$$

then for the decay of an initially pure K^0 or $\overline{K}^0$ state at a time $t = \tau$, we obtain from (3–4):

$$\begin{aligned} &\langle f|\ H_{wk}\ \left|K^0\right\rangle \\ &= \frac{(1-\varepsilon)}{\sqrt{2}}\left[(1+\delta)A_{fS}\mathrm{e}^{-\mathrm{i}\lambda_S\tau} + (1-\delta)A_{fL}\mathrm{e}^{-\mathrm{i}\lambda_L\tau}\right] , \\ &\langle f|\ H_{wk}\ \left|\overline{K}^0\right\rangle \\ &= \frac{(1+\varepsilon)}{\sqrt{2}}\left[(1-\delta)A_{fS}\mathrm{e}^{-\mathrm{i}\lambda_S\tau} - (1+\delta)A_{fL}\mathrm{e}^{-\mathrm{i}\lambda_L\tau}\right] , \end{aligned}$$

and the corresponding decay rates, $R(\overline{R}) = \left|\langle f|\ H_{wk}\ \left|\mathrm{K}^0(\overline{\mathrm{K}}^0)_{t=0}\right\rangle\right|^2$, are thus given by:

$$\begin{aligned}\frac{R(\tau)}{\overline{R}(\tau)} = \frac{[1 \mp 2\mathrm{Re}(\varepsilon)]}{2} \times \Big\{ &\big[1 \pm 2\mathrm{Re}(\delta)\big]|A_{f\mathrm{S}}|^2 \mathrm{e}^{-\Gamma_\mathrm{S}\tau} \\ &+\big[1 \mp 2\mathrm{Re}(\delta)\big]|A_{f\mathrm{L}}|^2 \mathrm{e}^{-\Gamma_\mathrm{L}\tau} \\ &\pm \mathrm{e}^{-\frac{1}{2}(\Gamma_\mathrm{S}+\Gamma_\mathrm{L})\tau}\Big(\big[1 \pm 2\mathrm{iIm}(\delta)\big] A^*_{f\mathrm{L}} A_{f\mathrm{S}} \mathrm{e}^{\mathrm{i}\Delta m\tau} \\ &+\big[1 \mp 2\mathrm{iIm}(\delta)\big] A^*_{f\mathrm{S}} A_{f\mathrm{L}} \mathrm{e}^{-\mathrm{i}\Delta m\tau} \Big) \Big\} .\end{aligned}$$

In the case of the decay to $\pi^+\pi^-(f \equiv \pi^+\pi^-)$ defining

$$\eta_{+-} \ = \ |\eta_{+-}|\mathrm{e}^{\mathrm{i}\phi_{+-}} \ = \ \frac{A_{f\mathrm{L}}}{A_{f\mathrm{S}}} \ = \ \frac{\langle \pi^+\pi^-|\ H_{wk}\ |\mathrm{K_L}\rangle}{\langle \pi^+\pi^-|\ H_{wk}\ |\mathrm{K_S}\rangle}, \quad (5)$$

where $|\eta_{+-}| \ll 1$, and $\Gamma_\mathrm{S}^{2\pi} = |A_{f\mathrm{S}}|^2$, the $\mathrm{K_S} \to \pi^+\pi^-$ partial width, we have

$$\begin{aligned}\frac{R(\tau)}{\overline{R}(\tau)} = \frac{[1 \mp 2\mathrm{Re}(\varepsilon - \delta)]}{2} \Gamma_\mathrm{S}^{2\pi} \times \big[&\mathrm{e}^{-\Gamma_\mathrm{S}\tau} + |\eta_{+-}|^2 \mathrm{e}^{-\Gamma_\mathrm{L}\tau} \\ &\pm 2|\eta_{+-}|\mathrm{e}^{-\frac{1}{2}(\Gamma_\mathrm{S}+\Gamma_\mathrm{L})\tau} \cos(\Delta m\tau - \phi_{+-})\big] . \quad (6)\end{aligned}$$

The interference term may be isolated by forming the decay-rate asymmetry

$$A_{+-}(\tau) = \frac{\overline{R}(\tau) - \alpha R(\tau)}{\overline{R}(\tau) + \alpha R(\tau)} , \quad (7)$$

with $\alpha = [1+2\mathrm{Re}(\varepsilon-\delta)]/[1-2\mathrm{Re}(\varepsilon-\delta)] = 1+4\mathrm{Re}(\varepsilon-\delta)$. We obtain:

$$A_{+-}(\tau) = -2\frac{|\eta_{+-}|\mathrm{e}^{\frac{1}{2}(\Gamma_\mathrm{S}-\Gamma_\mathrm{L})\tau} \cos(\Delta m\tau - \phi_{+-})}{1 + |\eta_{+-}|^2 \mathrm{e}^{(\Gamma_\mathrm{S}-\Gamma_\mathrm{L})\tau}} . \quad (8)$$

The use of this asymmetry to extract $|\eta_{+-}|$ and ϕ_{+-} from the CPLEAR data is discussed in detail in the next section.

3 Experimental method

In the CPLEAR experiment, the neutral kaons are produced by antiproton annihilation at rest in a high-pressure, gaseous hydrogen target via the reactions:

$$\mathrm{p\overline{p}} \ \to \ \begin{matrix} \mathrm{K^-\pi^+K^0} \\ \mathrm{K^+\pi^-\overline{K}^0} \end{matrix} \quad (9)$$

each of which has a branching ratio of $\approx 2\times10^{-3}$. The conservation of strangeness in the strong interaction dictates that a $\mathrm{K^0}$ is accompanied by a $\mathrm{K^-}$, and a $\overline{\mathrm{K}}^0$ by a $\mathrm{K^+}$. Hence, the strangeness of the neutral kaon at production is tagged by measuring the charge sign of the accompanying charged kaon.

For each initial strangeness, the numbers of neutral kaons decaying to $\pi^+\pi^-$, $N(\tau)$ and $\overline{N}(\tau)$, are measured as a function of the decay time τ, to form the asymmetry (7). However, the translation of measured numbers of events into decay rates requires (a) residual background, (b) acceptance factors which do not cancel in the asymmetry, and (c) regeneration effects to be taken into account.

(a) The amount of background, consisting of neutral-kaon semileptonic decays (see Sect. 6.3), depends on the decay time τ and is important, with respect to the $\pi^+\pi^-$ signal, only for late decay times. To a high degree of accuracy, the amount of background is the same for initial $\mathrm{K^0}$ and $\overline{\mathrm{K}}^0$ and hence cancels in the numerator, but not in the denominator, when using $\overline{N}(\tau)$ and $N(\tau)$ to construct the asymmetry, (7). Thus, the analytic expression for the asymmetry, (8), must be modified to

$$A^*_{+-}(\tau) \ = \ -2\frac{|\eta_{+-}|\mathrm{e}^{\frac{1}{2}(\Gamma_\mathrm{S}-\Gamma_\mathrm{L})\tau} \cos(\Delta m\tau - \phi_{+-})}{1 + [|\eta_{+-}|^2 + B(\tau)]\mathrm{e}^{(\Gamma_\mathrm{S}-\Gamma_\mathrm{L})\tau}} , \quad (10)$$

where $\Gamma_\mathrm{S}^{2\pi}B(\tau)\exp(-\Gamma_\mathrm{L}\tau)$ is the decay-time dependent background, from either $\mathrm{K^0}$ or $\overline{\mathrm{K}}^0$[1].

(b) The detection (tagging) efficiency of the $\mathrm{K^+\pi^-}$ and $\mathrm{K^-\pi^+}$ track-pairs, $\varepsilon(\mathrm{K^+\pi^-}) \equiv \varepsilon(\overline{\mathrm{K}}^0)$ and $\varepsilon(\mathrm{K^-\pi^+}) \equiv \varepsilon(\mathrm{K^0})$, respectively, are not the same, see Sect. 6.2. Hence, the measured number of $\mathrm{K^0}$ decays, $N(\tau)$, should be normalized to the measured number of $\overline{\mathrm{K}}^0$ decays, $\overline{N}(\tau)$, via a factor $\xi = \varepsilon(\mathrm{K^+\pi^-})/\varepsilon(\mathrm{K^-\pi^+})$. Since this factor depends on the kinematics of the event, we give each $\mathrm{K^0}$ event a weight dependent on the kinematics of the associated $\mathrm{K^\pm\pi^\mp}$ pair. As explained in Sect. 6.2, the quantity α is incorporated into the event weights. Effects related to a violation of charge symmetry in reactions (9) would be taken into account by this weighting procedure.

(c) The regeneration probabilities of $\mathrm{K^0}$ and $\overline{\mathrm{K}}^0$ propagating through the detector material are not the same, and this difference alters the measured ratio of $\overline{\mathrm{K}}^0$ to $\mathrm{K^0}$ decay events. This is corrected by giving each event a weight equal to the ratio of its decay probability when propagating in vacuum to that when traversing the detector, see Sect. 6.1 for details.

Hence, each $\mathrm{K^0}$ event is given a total weight equal to the product of the separate weights due to the relative normalization effects and regeneration, and the summed weight in each decay-time bin, $N_w(\tau)$, is computed. Each $\overline{\mathrm{K}}^0$ event is simply given a weight due to its regeneration correction and the corresponding summed weights, $\overline{N}_w(\tau)$, are determined. In the following $N_w(\tau)$ and $\overline{N}_w(\tau)$ are referred to as the *measured decay rates*. The measured asymmetry is then defined as

$$A^{\mathrm{exp}}_{+-}(\tau) \ = \ \frac{\overline{N}_w(\tau) - N_w(\tau)}{\overline{N}_w(\tau) + N_w(\tau)} . \quad (11)$$

[1] The additional term in the numerator, $2\mathrm{Re}(\delta)B(\tau)\exp[(\Gamma_\mathrm{S}-\Gamma_\mathrm{L})\tau]$, is completely negligible given the current limit on $\mathrm{Re}(\delta)$ [17]

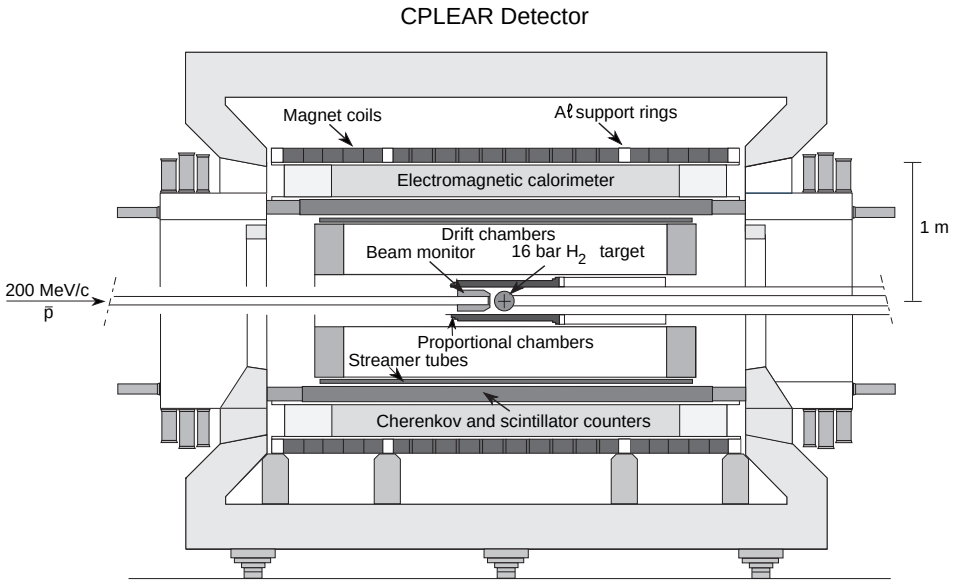

Fig. 1. A longitudinal view of the CPLEAR detector prior to mid 1994

To take account of statistical uncertainties in the normalization corrections and of correlations between the magnitudes of these corrections and the fitted CP-violation parameters, we allow the possibility of a further, overall normalization factor, k, multiplying $N_w(\tau)$. Thus, the asymmetry $A^*_{+-}(\tau)$, (10) , is set equal to $[\overline{N}_w(\tau) - kN_w(\tau)]/[\overline{N}_w(\tau)+kN_w(\tau)]$. Rearranging this, we see that the measured asymmetry, (11), is given by:

$$A^{\rm exp}_{+-}(\tau) = \frac{(k-1)+(k+1)A^*_{+-}(\tau)}{(k+1)+(k-1)A^*_{+-}(\tau)} \; . \qquad (12)$$

A fit is performed to the measured asymmetry using (12) with $|\eta_{+-}|$, ϕ_{+-} and k as free parameters.

In using (12) , we take advantage of the fact that the reactions (9) are strangeness conserving. A small strangeness violation (not expected at a level to be relevant here) would result in a dilution of the asymmetry and only affect $|\eta_{+-}|$.

4 The CPLEAR experiment

As explained above, the essence of the CPLEAR method is the selection of the desired antiproton annihilation channels, (9), from the dominating multipionic background and the identification of the neutral-kaon strangeness by measuring the charge sign of the accompanying charged kaon. For this, fast and efficient kaon identification is essential. Good particle identification is also necessary to distinguish between the various neutral-kaon decay channels. Decay-rate asymmetries must then be formed for neutral-kaon decay times up to $\approx 20\ \tau_{\rm S}$, where $\tau_{\rm S}$ is the $\rm K_S$ mean lifetime [3]. In order to accurately measure the desired parameters from the relevant asymmetries, very high statistics are necessary. Finally, in order to minimise neutral-kaon regeneration effects, the amount of material in the neutral-kaon decay volume must be kept to a minimum.

The above criteria determined the design of the CPLEAR detector, which is shown in Fig. 1. It had cylindrical geometry and was mounted inside a solenoid of length 3.6 m and internal radius 1 m, which produced a magnetic field of 0.44 T parallel to the antiproton beam. At the centre of the detector antiprotons, with a momentum of 200 MeV/c from the Low Energy Antiproton Ring (LEAR) at CERN, after crossing a degrader and a 1 mm scintillator (beam counter) were brought to rest and annihilated in a high-pressure gaseous hydrogen target. For data taken up to mid 1994 the target was a sphere of 7 cm radius at 16 bar pressure. After that date it was replaced by a 1.1 cm radius cylindrical target at 27 bar pressure. Identification of the charged kaon was performed by a threshold Cherenkov counter (C) sandwiched between two layers of plastic scintillator (S). The Cherenkov radiator, liquid FC72, was chosen to give efficient π/K separation in the momentum range (< 800 MeV/c) of charged particles in this experiment. The two scintillators were equipped with ADCs and the inner one with TDCs to give further particle identification via energy loss and time-of-flight information. This system provided fast information to the trigger for online kaon identification and was also used offline for π/K and π/e separation.

The tracking of charged particles, to determine their charge signs, their momenta and the positions of their production vertices, was performed by two proportional chambers, six drift chambers and two layers of streamer tubes. The total material in the target and tracking chambers amounted to $\approx 300\ {\rm mg}\cdot{\rm cm}^{-2}$ and $\approx 10^{-2}X_0$.

An electromagnetic calorimeter, consisting of eighteen layers of lead interleaved with high-gain streamer tubes, was used for photon detection and electron identification. The calorimeter had a total thickness of $\approx 6\,X_0$.

Due to the small branching ratio of the desired annihilation channels, (9), and the need for high statistics, it was necessary to run at high beam intensities ($\approx 10^6\ \overline{\rm p}/{\rm s}$). To cope with the high event rate and select the desired events

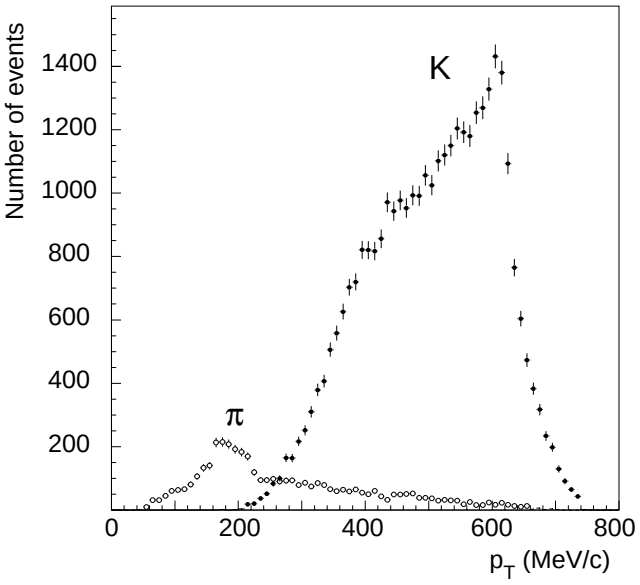

Fig. 2. p_{T} distribution for tracks with an S$\overline{\mathrm{C}}$S signature (simulated data, see text)

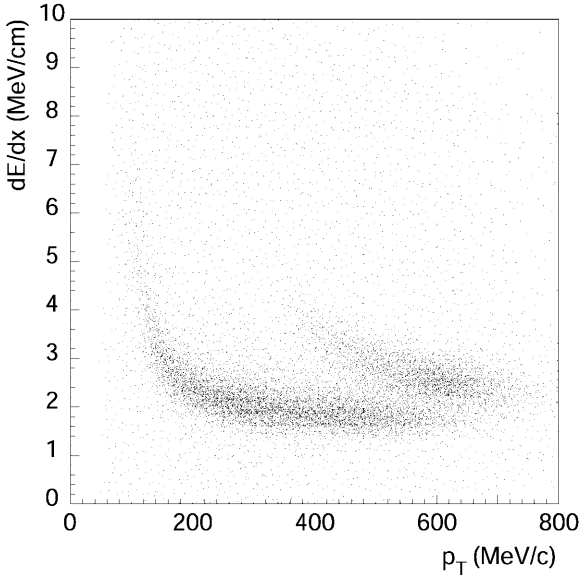

Fig. 3. $\mathrm{d}E/\mathrm{d}x$ in the inner scintillator vs p_{T} for all tracks (real data, see text)

from amongst the multipionic annihilations, a multilevel trigger was designed and built. It was based on custom-made hardwired processors which identified the charged kaon and reconstructed the event kinematics in $\approx 6\,\mu$s and gave an overall rejection factor of about 1000. The trigger was initiated by a $\overline{\mathrm{p}}$ signal in the beam counter, separated in time from any other $\overline{\mathrm{p}}$ by more than 90 ns and in coincidence with an S$\overline{\mathrm{C}}$S signal. The former condition, owing to the small cell size of the drift chambers, ensured that the probability of finding in the chambers track remnants from other annihilations was negligible.

For data taken from 1995 onwards, a cylindrical proportional chamber (PC0) of 1.5 cm radius, which had been installed together with the new target, was incorporated into the trigger. The decay of the neutral kaon outside this chamber was guaranteed by demanding not more than two hits in the chamber. This eliminated a large number of unwanted, very early decay-time $\mathrm{K_S}$ decays as well as background multikaon and multipion annihilations, and hence allowed the rate of useful events being recorded to be significantly increased.

A more detailed description of the CPLEAR detector and trigger system may be found in [18].

5 Event selection and comparison with simulated data

The selection of events corresponding to the desired annihilation channels followed by the decay of the neutral kaon to $\pi^+\pi^-$ is performed by a set of topological cuts and constrained fits. The same cuts are applied to both real and simulated data. The latter, owing to the high statistics (1.9×10^9 events), allow precise monitoring of efficiencies and losses in all selections.

5.1 Topological filter

In the first instance cuts are placed on the recorded events to verify that they correspond to the desired annihilation channels, (9). These demand that the event should contain either 2 or 4 charged-particle tracks with zero total charge. Cuts are placed on the quality of each track and the requirement is made of at least one charged-kaon candidate, defined as a track giving an S$\overline{\mathrm{C}}$S signature from the scintillator-Cherenkov-scintillator sandwich and having a momentum component (p_{T}) in the transverse plane greater than 300 MeV/c. Figure 2 shows the p_{T} distribution of tracks having an S$\overline{\mathrm{C}}$S signature in simulated data. It can be seen that tracks below 300 MeV/c are almost exclusively pions, while those above 300 MeV/c are almost exclusively kaons. At least one kaon candidate is required to have an energy loss, $\mathrm{d}E/\mathrm{d}x$, in the inner scintillator, S_1, consistent with that predicted by the Bethe-Bloch formula for a kaon having the measured momentum of this track. The $\mathrm{d}E/\mathrm{d}x$ distribution in S_1 versus p_{T} is shown for all tracks in all events, selected with the criteria mentioned earlier, in Fig. 3. This shows two distinct bands corresponding to pions and kaons, thus enabling a good separation of these particles above 300 MeV/c. Finally, it is demanded that a satisfactory vertex, well within the target volume, be formed between at least one kaon candidate and an oppositely-charged track (primary vertex).

For the selection of neutral kaons decaying to $\pi^+\pi^-$, further topological cuts are applied. These are:

- four charged-particle tracks in the event, including one surviving kaon candidate, which must have a total momentum of at least 350 MeV/c.
- the charged kaon and associated (primary) pion, found in the offline analysis, must be the same tracks as those used online to satisfy the trigger conditions.

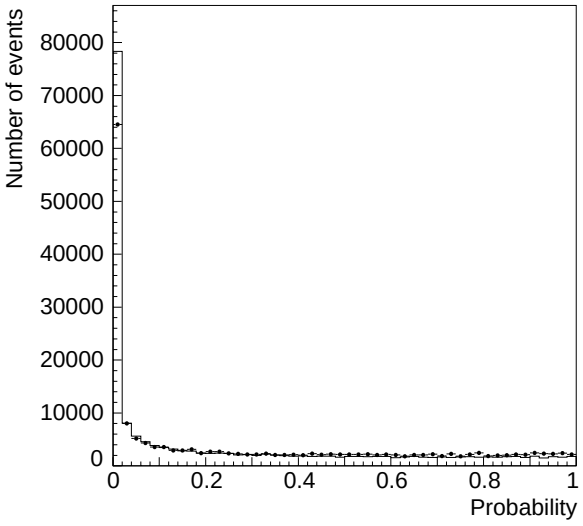

Fig. 4. 1C-fit probability distribution for real (–) and simulated (•) data

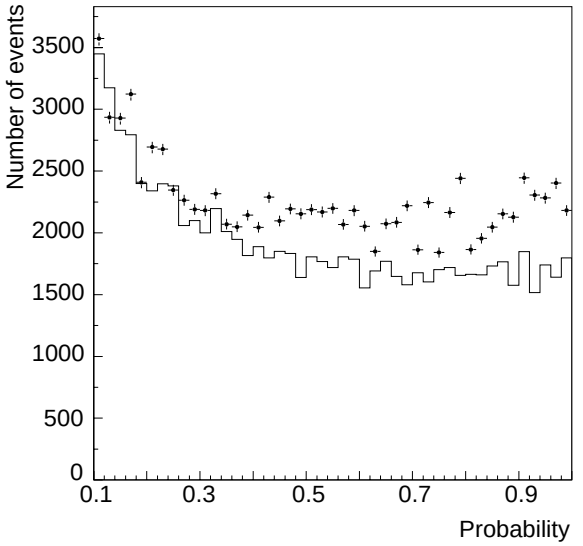

Fig. 5. 1C-fit probability distribution for real (–) and simulated (+) data above 10% probability

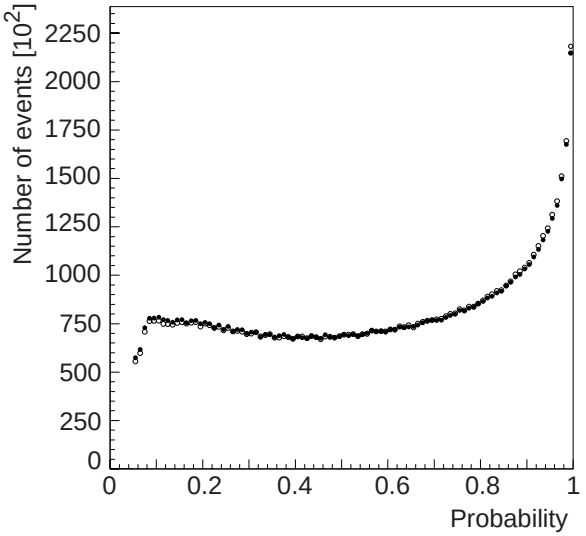

Fig. 6. 9C-fit probability distribution from real data for initial K^0 (•) and $\overline{K}^0$ (○)

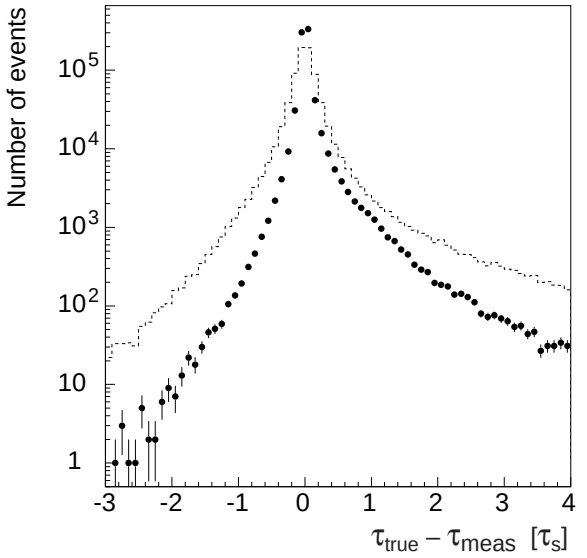

Fig. 7. Distribution of the difference between true and measured decay time, from track fit (–) and 9C fit (•) of simulated data

– the track with the same charge sign as the kaon candidate must form a satisfactory vertex with the remaining opposite-sign track (secondary vertex). For data taken with PC0 in the trigger, this vertex must lie outside the radius of this chamber.
– no track should have an unphysical fitted momentum, i.e. less than 60 MeV/c, below which the track would not reach S_1, or above 1 GeV/c.
– the opening angles between the two tracks at both primary and secondary vertices should lie between 11° and 169°.

The second condition, 'track matching', ensures that no event survives where the trigger conditions were satisfied by tracks other than the *true* primary Kπ pair. The final requirement removes events where the vertex position is poorly known due to tracks being almost parallel or back-to-back. It also removes backscatter events and photon conversions.

5.2 Constrained fits

In order to further reduce background from other annihilation channels and from other decay channels of the neutral kaon, a series of constrained fits are applied to the events which survive the topological cuts. These fits have the additional advantage that they considerably improve the decay-time resolution of the neutral kaon. The constrained fits applied are as follows:

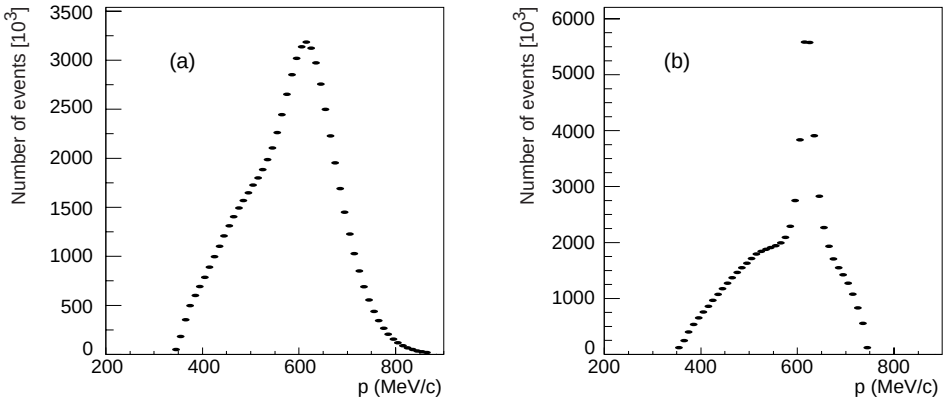

Fig. 8a,b. Charged-kaon momentum distribution for real data after **a** track fit and **b** 9C fit

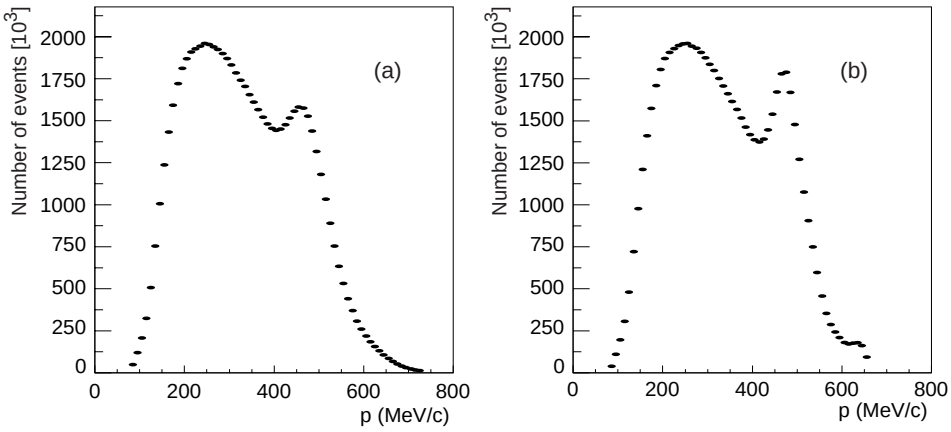

Fig. 9a,b. Primary-pion momentum distribution for real data after **a** track fit and **b** 9C fit

- 1C fit. This imposes the constraint that the missing mass at the primary vertex should equal the neutral-kaon mass.
- 4C fit. This imposes the constraints of overall energy and momentum conservation.
- 5C fit. This is an extension of the 4C fit with the additional constraint that the invariant mass at the secondary vertex should equal the neutral-kaon mass.
- 9C fit. This combines the 4C and 1C fits with the additional constraints that:
  - at each vertex, corresponding to the intersection of the two tracks in the transverse plane, the two tracks should also have the same coordinate along the beam axis (2C).
  - the neutral-kaon momentum should be colinear, in both transverse and longitudinal planes, with the line joining the two vertices (2C).

Figures 4 and 5 show the probability distribution for the 1C fit for both real data and $\pi^+\pi^-$ Monte Carlo, normalized to the same total number of events. It can be seen that there are more data events with low probability and correspondingly more Monte Carlo events with high probability. This is because the data contains background events from other annihilation channels. A cut is placed on this probability at 2.5% and on the 5C-fit probability at 5%. A 5% cut is also placed on the 9C-fit probability. In order to keep the background/signal ratio below unity, tighter cuts are applied to the 9C-fit probability at late decay times. The probability cut increases from 5% at 11 τ_S to $\approx 60\%$ beyond 17 τ_S.

The difference in probability distributions between real and simulated data (Fig. 5) is not important as the final results have very little dependence on the use of simulated data. Its only use is in the determination of the neutral-kaon decay-time resolution correction and of the decay-time dependence of the background/signal ratio. The final results have only weak sensitivity to both these quantities (see Sect. 7.2). What is important, however, is that the probability distributions should be the same for initial K^0 and $\overline{K}^0$. This is demonstrated in Fig. 6, where the 9C-fit probability distribution, after the cut at 5%, is shown for K^0 and $\overline{K}^0$ separately. It can be seen that the two are the same within a few per cent. The slight difference between these distributions is taken care of by the normalization procedure between K^0 and $\overline{K}^0$. The effect of any residual difference is then described by the systematic uncertainties on the fitted quantities due to the variation in the cut on the 9C-fit probability (see Sect. 7.2).

The improvement in the neutral-kaon decay-time resolution as a result of the constrained fits can be seen in Fig. 7. Here, using simulated data, the difference is histogrammed between the true neutral-kaon decay time and its measured value, using the track-fit value and the value from the 9C fit. This improvement is largely due to an improvement in the momentum resolution of the primary charged tracks and, hence, of the neutral kaon. This is demonstrated in Figs. 8a and 8b, 9a and 9b, 10a and 10b.

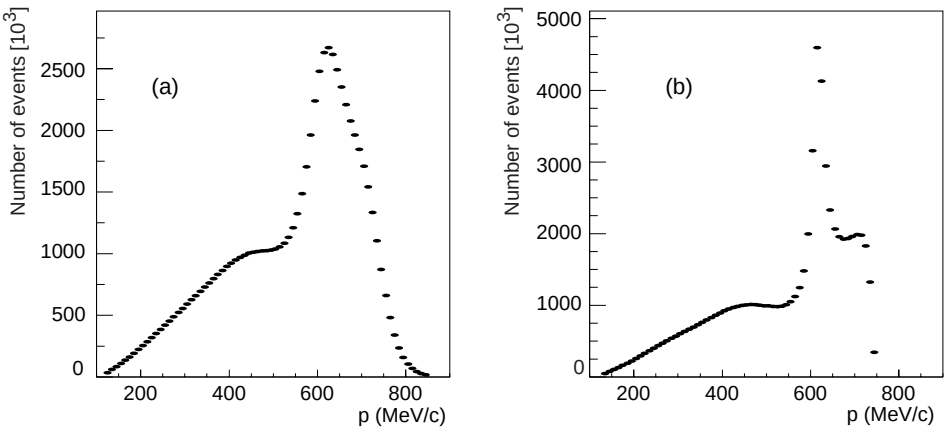

Fig. 10a,b. Neutral-kaon momentum distribution for real data after **a** track fit and **b** 9C fit

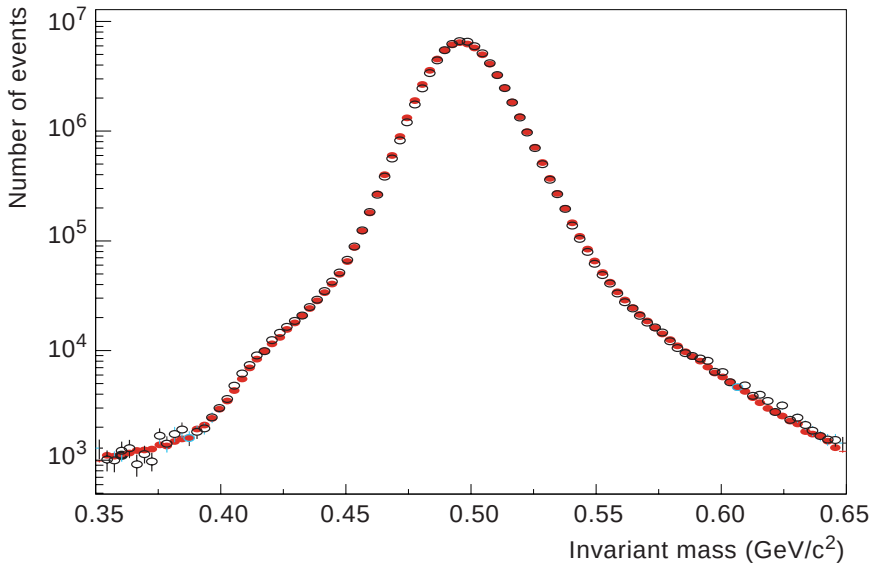

Fig. 11. Invariant mass at the secondary vertex for real (•) and simulated (○) data

These show respectively the charged-kaon, primary-pion and neutral-kaon momentum distributions from real data, using the track-fit values, (a), and the 9C-fit values, (b). The peak in the charged-kaon momentum distribution is due to $p\overline{p}$ annihilation into $K^{\pm}K^*(892)^{\mp}$ with subsequent decay of the $K^*(892)^{\pm}$ to charged pion and neutral kaon. That in the primary pion distribution is due to annihilation into $\pi^{\pm}a_2(1320)^{\mp}$ with subsequent decay of the $a_2(1320)^{\pm}$ into charged kaon plus neutral kaon. Finally, that in the neutral-kaon distribution is due to annihilation into $K^0\overline{K}^*(892)^0$ and $\overline{K}^0K^*(892)^0$ with subsequent decay of the neutral K^* into charged kaon and charged pion. In all cases the decays of these resonances, being due to the strong interaction, conserve strangeness and so do not affect the event tagging. The improvement in the mass resolution of all resonances due to the constrained fit is clear to see. After the 9C fit, studies of simulated data show that the neutral-kaon decay-time resolution varies from 0.05 τ_S at early decay times to 0.11 τ_S at late decay times.

The simulation quality is demonstrated by Fig. 11 which shows the invariant mass of the two particles at the secondary vertex, for real and simulated data, after all cuts. This has been calculated using the track-fit momenta and shows excellent agreement, over four orders of magnitude, between real and simulated data.

A total of 7.0×10^7 events having a measured decay time above 1 τ_S survive this selection procedure, with an estimated residual background of 0.05%. The corrections which need to be applied to the measured numbers of K^0 and $\overline{K}^0$ events prior to forming the asymmetry, $A_{+-}^{\exp}(\tau)$, and the determination of the residual background level are discussed in the next section.

6 Decay-rate corrections and background determination

6.1 Regeneration

The measured numbers of K^0 and $\overline{K}^0$ events must be corrected for both coherent and incoherent regeneration. These arise from interference between the inherent K_S amplitude of the neutral kaon and that regenerated from the K_L amplitude by scattering in the detector material. This correction is performed by giving each event a weight,

equal to the ratio of its decay probability when propagating in vacuum to that when traversing the detector. These weights, for neutral-kaon momenta between 550 and 650 MeV/c and decay times in the interval $1-10\ \tau_S$, lie in the range 0.969 to 1.010 for K^0, and 0.992 to 1.004 for $\overline{K}^0$. At later decay times they range from 1.0 to 0.9 for both K^0 and $\overline{K}^0$.

This ratio depends on the magnitude and direction of the neutral-kaon momentum and on the positions of its production and decay vertices and requires an accurate description of all the detector materials traversed by the neutral kaon. It also requires knowledge of the forward scattering amplitudes of K^0 and $\overline{K}^0$ which are strongly momentum dependent. In an earlier paper [11], due to lack of knowledge of the amplitudes in the momentum range of this experiment (< 800 MeV/c), we used the calculated values of Eberhard and Uchiyama [19]. During dedicated data-taking in 1996, a carbon regenerator was inserted into the detector, enabling us to measure these amplitudes [20]. The measured values were in good agreement with the earlier calculations but have enabled us to reduce the systematic error on the size of the regeneration correction by a factor of more than three.

The semileptonic background is essentially not affected by the regeneration. Thus, once the level of background as a function of the neutral-kaon decay time is known (see Sect. 6.3), the regeneration weight, mentioned above, is corrected for the fraction of background at the decay time of each event. This correction changes the sizes of the regeneration corrections to the fitted results, by only about 10% of their estimated uncertainties. This is because at early decay times where regeneration effects are significant, the fraction of background is very small, whereas at later decay times, where the background fraction is large, the effect of regeneration corrections on the final fitted results is extremely small.

Separate regeneration corrections were calculated for the two hydrogen targets. For data taken with the original, 16 bar target, coherent regeneration increases the value of ϕ_{+-} by 3.5° and reduces the value of $|\eta_{+-}|$ by 0.08×10^{-3}. For data taken with the 27 bar target the corrections are smaller due to the smaller distance of the target wall from the production vertex, ϕ_{+-} being increased by 2.6° and $|\eta_{+-}|$ being reduced by 0.05×10^{-3}. The effects of incoherent regeneration are much smaller, reducing ϕ_{+-} by 0.11° and $|\eta_{+-}|$ by 0.003×10^{-3} for both targets. The errors on the sizes of these corrections are discussed in Sect. 7.2.

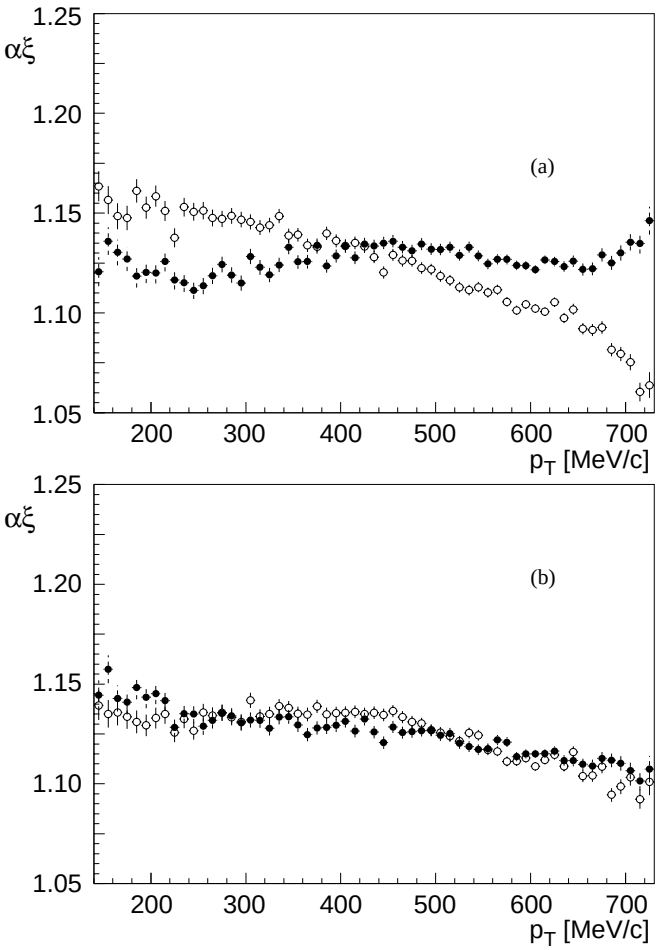

Fig. 12a,b. The dependence of $\alpha\xi$ on the neutral-kaon transverse momentum p_T, when **a** K^0 and $\overline{K}^0$ events are measured with the same magnetic-field polarity, positive (○) or negative (●), and **b** K^0 and $\overline{K}^0$ events are measured with opposite field polarities, so that the charged kaons have the same curvature sign, positive (○) or negative (●)

6.2 Normalization of K^0 and $\overline{K}^0$ decay rates

As mentioned in Sect. 3, the detection efficiencies of the $K^-\pi^+$ and $K^+\pi^-$ pairs, used to tag K^0 and $\overline{K}^0$ production, $\varepsilon(K^-\pi^+)$ and $\varepsilon(K^+\pi^-)$, respectively, are not the same, and $\xi = \varepsilon(K^+\pi^-)/\varepsilon(K^-\pi^+)$ differs from unity. Since the efficiency of detecting a $\pi^+\pi^-$ pair from a K^0 decay is the same as that from a $\overline{K}^0$ decay, ξ is also the ratio of the acceptances of initial $\overline{K}^0$ and K^0 decaying to $\pi^+\pi^-$. This difference in the $K\pi$ detection efficiencies has two sources:

- slight geometrical imperfections in the detector which cause the detection efficiency of a track to depend on its curvature sign. This also arises from biases introduced by the trigger, which assumes, for example, that all particles originate from the centre of the detector.
- differences in the strong interaction probabilities of K^+ and K^-, and of π^+ and π^-, with the detector material (principally the scintillators and Cherenkov counter).

Neither of the above effects can be modelled with sufficient accuracy to enable ξ to be determined from simulated data. It is thus determined from real data using events with decay times between 1 and 4 τ_S, where statistics are high, the proportion of background events is negligible (see Sect. 6.3) and CP violation effects are small. In this decay-time range, for a bin of $K\pi$ kinematical configurations, $\mathbf{p}_K, \mathbf{p}_\pi$, we obtain from (6), denoting by N_1 and $\overline{N}_1$ the summed regeneration weights of K^0 and $\overline{K}^0$ decays,

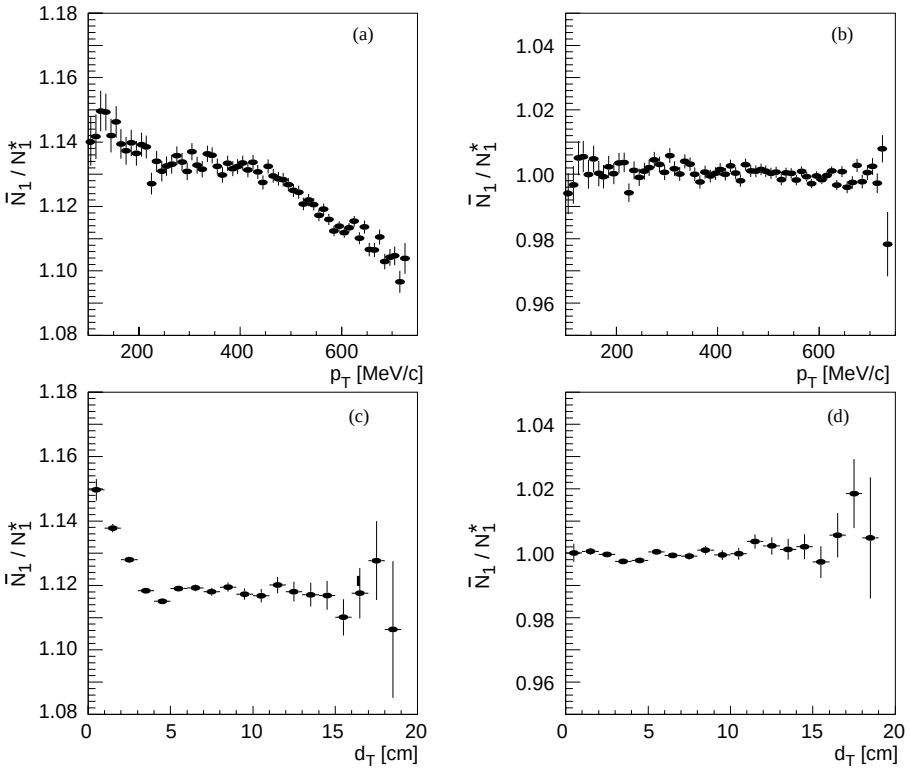

Fig. 13a–d. The ratios $\overline{N}_1(p_T)/N_1^*(p_T)$ versus the neutral-kaon transverse momentum p_T **a** before and **b** after giving each K^0 event its normalization weight, and $\overline{N}_1(d_T)/N_1^*(d_T)$ versus the vertex transverse separation d_T **c** before and **d** after giving each K^0 event its normalization weight. Note that the quantity displayed in **a** is in fact $\alpha\xi(p_T)$ for data summed over the two field polarities

$$[1+4\mathrm{Re}(\varepsilon-\delta)]\xi(\mathbf{p}_K,\mathbf{p}_\pi)\frac{N_1(\tau|\,\mathbf{p}_K,\mathbf{p}_\pi)}{\overline{N}_1(\tau|\,\mathbf{p}_K,\mathbf{p}_\pi)} \approx \left(1+4|\eta_{+-}|e^{\frac{1}{2}\Gamma_S\tau}\cos(\Delta m\tau-\phi_{+-})\right).$$

Since ξ depends only on the kinematics of the primary $K\pi$ pair, it has the same value for all decay times. Hence, summing over all the decay times between 1 and 4 τ_S, we have

$$\alpha\xi(\mathbf{p}_K,\mathbf{p}_\pi) \equiv [1+4\mathrm{Re}(\varepsilon-\delta)]\xi(\mathbf{p}_K,\mathbf{p}_\pi) \quad (13a)$$

$$= \frac{\sum \overline{N}_1(\tau|\,\mathbf{p}_K,\mathbf{p}_\pi)}{\sum N_1(\tau|\,\mathbf{p}_K,\mathbf{p}_\pi)\big(1-f(\tau)\big)}\,, \quad (13b)$$

where $f(\tau)=4|\eta_{+-}|e^{\frac{1}{2}\Gamma_S\tau}\cos(\Delta m\tau-\phi_{+-})$. In this decay-time range, using world-average values [3] for the relevant parameters, the CP-violation term, $f(\tau)$, is always less than 0.04 and is known to a precision of one part in 10^4. The dependence of $\alpha\xi$ on any other $K\pi$-pair kinematical variables is simply obtained from (13) by binning the neutral kaons in those variables, as for instance in Fig. 12.

Figure 12 illustrates the biases arising from curvature-dependent efficiencies mentioned above. In Fig. 12a the quantity $\alpha\xi(p_T)$ is shown for each magnetic-field polarity separately, as a function of the neutral-kaon transverse momentum component, p_T, and large differences are evident, due to the track-curvature dependence of the tagging efficiency. In Fig. 12b the same quantity is shown for each curvature sign of the charged kaon, i.e. $\alpha\xi(p_T)$ is built with the number of $\overline{K}^0$ events for one field polarity divided by the number of K^0 events for the other. It can be seen that the two ratios are now the same to within a few parts per mil over the entire p_T range. This shows that, for a given curvature of the charged tracks, geometrical biases are identical for $\overline{K}^0$ and K^0 events and cancel in the ratio. These biases are eliminated by frequent reversals of the field polarity, every eight hours under steady data-taking conditions, so that equal amounts of data are taken with each field polarity. Studies using high-statistics, simulated data have shown that such curvature-dependent biases can be completely eliminated by adding the data from the two field polarities. The K^0 and $\overline{K}^0$ data samples to which we refer in the following are the result of such addition.

Figure 12b shows, as expected, a dependence of $\alpha\xi$ on the neutral-kaon p_T, resulting from the dependence of the primary $K^\pm\pi^\mp$ strong interaction probabilities on their kinematics, to which the neutral-kaon p_T is correlated. This leads to a dependence of ξ on the neutral-kaon decay time, due to the correlation between its momentum and decay time, which, in turn, is a consequence of the finite decay volume of the detector: those neutral kaons with high momentum decaying on average at earlier times than those with low momentum. However, as explained above, for a given primary $K\pi$ kinematics the detection efficiency is the same at all decay times. Hence, a multi-dimensional table of event weights, in bins of the relevant $K\pi$ kinematic variables, is constructed, according to (13). In practice, it is adequate to produce the table of event weights in only a subset of these variables, namely transverse and longitudinal components of the charged-kaon momentum, p_K^t and p_K^ℓ, and magnitude of the primary-pion momentum p_π. The quantity which is directly determined from (13) is $[1+4\mathrm{Re}(\varepsilon-\delta)]\xi(p_K^t,p_K^\ell,p_\pi) \equiv \alpha\xi(p_K^t,p_K^\ell,p_\pi)$. This quantity is determined in bins of the primary $K\pi$ variables and

applied as a weight to the K^0 decays on an event-by-event basis, α being included in the event weights without explicitly needing to know its value. In a first iteration, the world-average values [3] for the CP parameters are used to calculate $f(\tau)$, and the corresponding summed weights enter the fit procedure of Sect. 7. In a second iteration, we use the values given by the fit. The fit results have very little sensitivity to the values of these CP parameters, and there is no change in the fit values after the first iteration. The final summed weights of K^0 and $\overline{K}^0$ events are denoted by N_w and $\overline{N}_w$.

The effectiveness of the method is illustrated in Fig. 13 with respect to the neutral-kaon transverse momentum p_T and the separation of its production and decay vertices in the transverse plane, d_T, the two variables used in the determination of the neutral-kaon decay time. Summing the number of decays in a p_T bin, over all the decay times in the $1-4$ τ_S range, we plot in Fig. 13a the ratio $\overline{N}_1(p_T)/N_1^*(p_T)$, where $\overline{N}_1(p_T) \equiv \sum \overline{N}_1(\tau|\, p_T)$ and $N_1^*(p_T) \equiv \sum N_1(\tau|\, p_T)(1-f(\tau))$, and in Fig. 13b the corresponding ratio after giving each K^0 event its normalization weight, that is building the denominator from $N_w(\tau|\, p_T)$ instead of $N_1(\tau|\, p_T)$. Figures 13c and d are the corresponding plots where the data are binned as a function of d_T rather than p_T. The value of the overall normalization factor k (see Sect. 3), left free in the fit of (12) to the data, (11), over the whole measured decay-time range, is determined to be 0.9997 ± 0.0004.

6.3 Background determination

Studies using high-statistics simulated data show that the only remaining source of background events in the real data, following the cuts detailed in Sect. 5, is semileptonic decays of K_L. As can be seen from (10), the quantity which is required to describe the background in the asymmetry is $B(\tau)/|\eta_{+-}|^2$, which is just the ratio of the K_L semileptonic background to the CP-violating $K_L \to \pi^+\pi^-$ signal. The dependence of this ratio on the neutral-kaon decay time is determined from simulated data and is shown in Fig. 14. Note that the overall background/signal ratio at late decay times, where K_S decays are negligible, is the same as that shown in the figure. But, at earlier decay times, the overall background/signal ratio is much less than that shown, since the signal is dominated by K_S decays.

The rapid decrease in background level between 11 and 14 τ_S is due to the tighter 9C-fit probability cuts applied at decay times beyond 11 τ_S, designed to keep the background/signal ratio at late decay times to about unity (see Sect. 5.2). The curve shown is a fit to the simulated data, parametrising them with a 5th order polynomial below 11 τ_S and a 3rd order polynomial above 11 τ_S. This parametrisation of the background decay-time dependence is used in the fit to the experimental asymmetry with (12). The absolute level of background at any decay time is determined by three independent methods:

– from the relative acceptance of semileptonic and $\pi^+\pi^-$ data and the known branching ratios for neutral kaons decaying to these final states. This is the method used to produce Fig. 14.
– from a fit to the experimental decay rate for the sum of K^0 plus $\overline{K}^0$ after correction for the decay-time dependence of the common acceptance.
– by leaving the background level as a free parameter in the fit to the experimental asymmetry with (12).

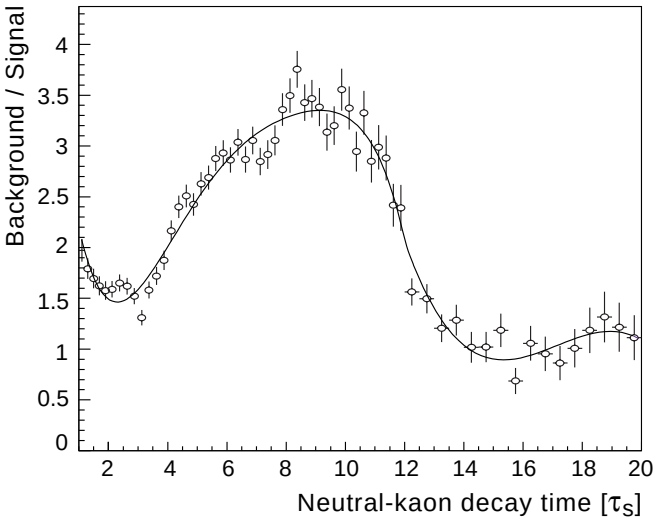

Fig. 14. Ratio of K_L background to K_L signal ($K_L \to \pi^+\pi^-$). The continuous curve is a parametrised fit to the simulated data (○)

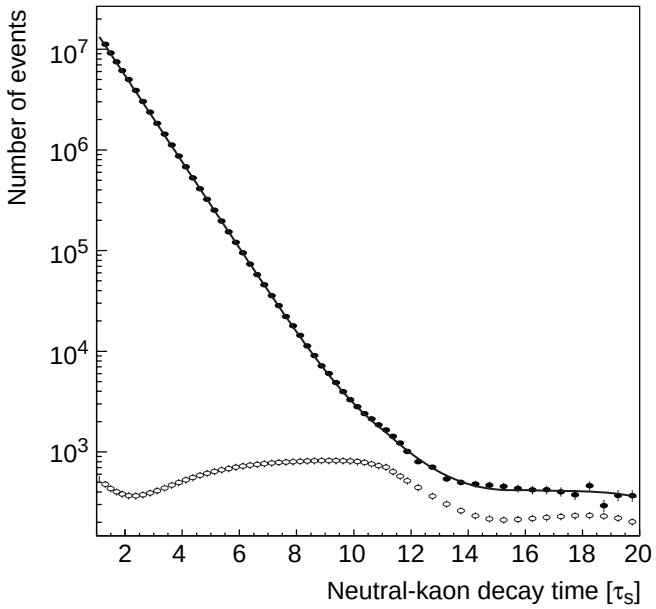

Fig. 15. The measured decay rate (acceptance corrected) for K^0 plus $\overline{K}^0$. The continuous curve is a fit to the real data (●). The open circles show the calculated background level

The second method is illustrated in Fig. 15, which shows the measured (K^0 plus $\overline{K}^0$) decay rate, corrected for acceptance. With the decay-time dependence of the background fixed by the parametrisation described above, a 3-parameter fit to the data is performed. The free pa-

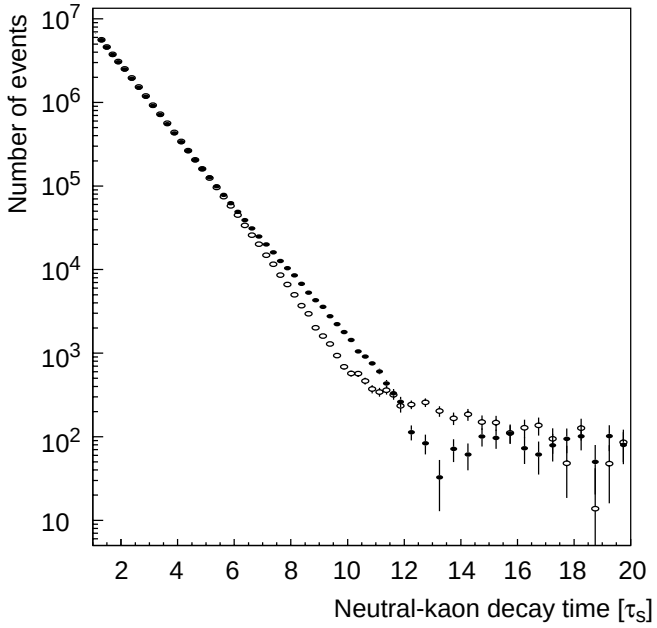

Fig. 16. The measured decay rates for K^0 (○) and $\overline{K}^0$ (●) after acceptance correction and background subtraction

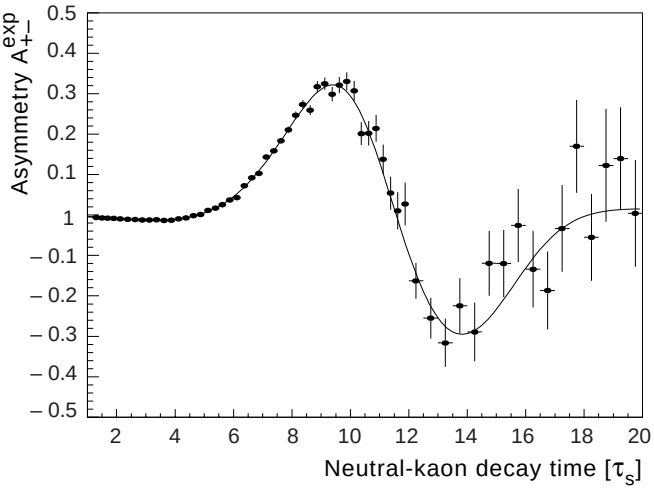

Fig. 17. The measured decay-rate asymmetry, $A_{+-}^{\rm exp}(\tau)$. The solid circles are the data points, including residual background, while the continuous curve is the result of our fit

rameters are the background absolute level, the K_S mean lifetime and the intercept at $\tau = 0$. The result of the fit is shown by the continuous curve. The value obtained for the K_S mean lifetime agrees with the world-average value to within 1%, the precision expected from the accuracy to which the absolute acceptance of the detector is known. This uncertainty on the absolute acceptance does not affect the fit to the experimental asymmetry with (12), since the $\pi^+\pi^-$ acceptance cancels between numerator and denominator. Only the ratio of the semileptonic to $\pi^+\pi^-$ acceptances enters, through the decay-time dependence of the background.

In the third method, the decay-time dependence of the background is once again fixed as above but its absolute level is left as a free parameter in the fit to the experimental asymmetry with (12). The three methods yield values in good agreement with each other. The absolute level of the background is then fixed to the mean value obtained from the three methods.

7 Results

The two rates $R(\tau)$ and $\overline{R}(\tau)$, (6), are the decay rates of CP conjugate states. Hence any difference between them is direct evidence of CP violation. The measured decay rates, as defined in Sect. 3, are displayed separately, for initial K^0 and $\overline{K}^0$, in Fig. 16, after acceptance correction and background subtraction, and clearly show the expected CP-violation effect.

The measured decay-rate asymmetry, (11), is shown in Fig. 17 and is fitted by (12) with ϕ_{+-}, $|\eta_{+-}|$, and k as free parameters. The decay-time dependence of the background, $B(\tau)$, is fixed to the parametrisation described in Sect. 6.3 and its absolute level to the mean value obtained from the three methods above. The values of Γ_L and Γ_S are fixed to the world-average values [3], as also, normally, is the value of Δm. Fits have also been performed with Δm as an additional free parameter.

Table 1. Correlation coefficients for the fitted values in the case of fixed Δm

	ϕ_{+-}	$\lvert\eta_{+-}\rvert$	k
ϕ_{+-}	1	0.17	0.37
$\lvert\eta_{+-}\rvert$	-	1	0.65
k		-	1

The value obtained for ϕ_{+-} depends on the value of Δm, varying as

$$\phi_{+-}^{\Delta m} = \phi_{+-}^{\langle\Delta m\rangle} + 0.300(\Delta m\ - \langle\Delta m\rangle),$$

with ϕ_{+-} in degrees and Δm in units of $10^7\hbar s^{-1}$, but has negligible dependence on the value of τ_S. The value of $|\eta_{+-}|$ depends on the value of τ_S as

$$|\eta_{+-}|^{\tau_S} = |\eta_{+-}|^{\langle\tau_S\rangle} + 0.091(\tau_S\ - \langle\tau_S\rangle) \times 10^{-3},$$

where τ_S is in ps, and has negligible dependence on the value of Δm. Neither $|\eta_{+-}|$ nor ϕ_{+-} have any significant dependence on the value of Γ_L used in the fit.

Using for $\langle\Delta m\rangle$ and $\langle\tau_S\rangle$ the world averages [3], $\langle\Delta m\rangle = (530.1 \pm 1.4) \times 10^7\hbar s^{-1}$ and $\langle\tau_S\rangle = (89.34 \pm 0.08)$ ps, the results of the fit are:

$$|\eta_{+-}| = (2.264 \pm 0.023) \times 10^{-3}\ ,$$
$$\phi_{+-} = 43.19^\circ \pm 0.53^\circ\ ,$$
$$k = 0.9997 \pm 0.0004\ ,$$

where the errors are purely statistical and $\chi^2/\text{d.o.f.} = 1.2$. The result of the fit is shown as a solid line in Fig. 17. Table 1 shows the correlation coefficients between ϕ_{+-}, $|\eta_{+-}|$ and k, given by the fit.

An alternative way of presenting the data is given by the 'reduced asymmetry', $A_{\rm red}(\tau) = A_{+-}^{\rm exp}(\tau)\times$

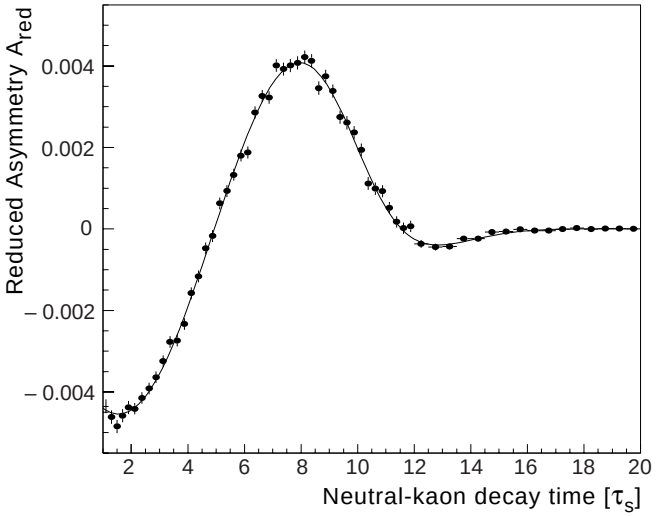

Fig. 18. The 'reduced asymmetry' $A_{\rm red}(\tau)$ (see text). The continuous curve is calculated from the result of our fit

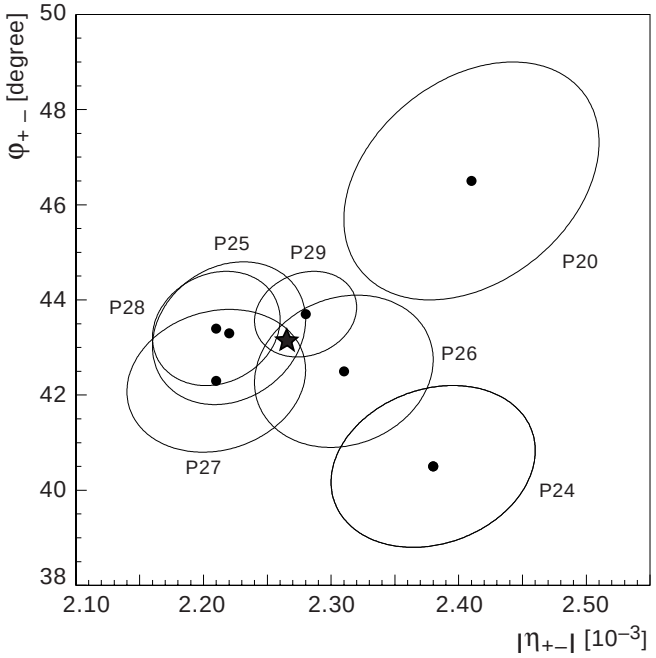

Fig. 19. The one-sigma error ellipses for ϕ_{+-} versus $|\eta_{+-}|$ for each data-taking period (P20, P24-P29). The final result (★) is also shown

$e^{-\frac{1}{2}(\Gamma_S-\Gamma_L)\tau}$, as shown in Fig. 18[2]. The physics content of Fig. 18 is identical to that of Fig. 17, but it emphasizes the low/medium decay-time region where statistics are high and to which the fit is sensitive, at the expense of the high decay-time region where statistics are low and to which the fit has little or no sensitivity.

If the value of Δm is left free in the fit, the result is $\Delta m = (524.0 \pm 4.4_{\rm stat} \pm 3.3_{\rm syst}) \times 10^7 \hbar {\rm s}^{-1}$, in agreement with the value $(529.5 \pm 2.0_{\rm stat} \pm 0.3_{\rm syst}) \times 10^7 \hbar {\rm s}^{-1}$ obtained from the complete sample of CPLEAR semileptonic data [21]; the correlation coefficient between Δm and ϕ_{+-} is 0.92. The systematic errors of this Δm measurement are discussed in Sect. 7.2.

7.1 Consistency of results

The data presented in this paper were taken in a number of separate data-taking periods between 1992 and 1995, data-taking in 1996 being devoted to special running to measure the neutral-kaon forward scattering amplitudes. To check the internal consistency of the data, fits were performed for each data-taking period separately. The results are shown in Fig. 19, together with the one-standard deviation error ellipses of ϕ_{+-} versus $|\eta_{+-}|$, taking into account their correlations. The value of the overall χ^2 is 10.3 for 12 d.o.f., showing that the results for each period are internally consistent within their statistical errors.

7.2 Systematic errors

The following sources of systematic error have been investigated:

– background level and decay-time dependence,
– changes in cut values,
– neutral-kaon decay-time resolution,
– normalization procedure,
– absolute time measurement,
– regeneration correction.

As mentioned above, the level of background is fixed to the mean value of its three separate determinations. The scatter of these values indicates an uncertainty on this mean level of 6%. The uncertainty on the decay-time dependence of the background is determined from the errors on the parameters obtained from the fit shown in Fig. 14. By varying both the level and decay-time dependence of the background within their estimated uncertainties, the corresponding systematic errors on the fitted parameters are determined.

The level and decay-time dependence of the background at late decay times can be varied by changing the values of the 9C-fit probability cuts at these decay times (see Sect. 5.2). These changes in background level and shape lead to small variations in the values of the fitted parameters. This is particularly true for Δm which has much greater sensitivity than ϕ_{+-} or $|\eta_{+-}|$ to data beyond $10-12\ \tau_S$. The values of other cuts have also been varied and found to give very small changes in the values of the fitted parameters. The magnitudes of the variations of the fitted parameter values due to changes in cuts are taken as additional sources of systematic error.

The measured values of ϕ_{+-}, $|\eta_{+-}|$ and Δm, stated earlier, have already been corrected for the finite resolution of the neutral-kaon decay-time measurement. The sizes of these corrections, determined using high-statistics simulated data, are $-0.18°$, $+0.042 \times 10^{-3}$ and $+0.7 \times 10^7 \hbar {\rm s}^{-1}$ respectively. The systematic errors due to these

[2] It should be noted that the corresponding plot in [2] has a factor of two error in the vertical scale. What is actually shown in [2] is $0.5 \times A_{\rm red}(\tau)$

corrections are obtained by varying the resolution correction, as a function of decay time, by its uncertainty, due to the finite statistics of the simulated data.

The normalization procedure of applying event weights changes the fitted value of ϕ_{+-} by $+0.65°$, of $|\eta_{+-}|$ by $+0.02\times10^{-3}$ and of Δm by $-1.3\times10^{7}\hbar\mathrm{s}^{-1}$. To determine the systematic errors induced by the normalization procedure, a large number of different event-weight tables were constructed in which the correction factors were varied randomly within their statistical uncertainties. The systematic errors on the fitted parameters were then taken to be the standard deviations of the distributions of the corresponding changes in their values due to the different event weighting.

Extensive studies have shown that after the kinematic constrained fit, the absolute time scale measured in the experiment is known with a precision of ±0.2 parts per mil [18,22]. Changing the absolute time scale by this factor produces the shifts in the fitted parameters shown in Table 2.

The systematic uncertainties on the regeneration corrections have been determined by varying both the real and imaginary parts of the neutral-kaon forward scattering amplitudes by their combined statistical and systematic uncertainties. Contributions to the systematic errors due to uncertainties in the positions, thicknesses and densities of the various elements of the detector traversed by the neutral kaons were found to be negligible.

The values of all sources of systematic error on ϕ_{+-} and $|\eta_{+-}|$ are shown in Table 2 for Δm fixed. The errors arising from $\langle\Delta m\rangle$ and $\langle\tau_S\rangle$ are calculated from the quoted corresponding uncertainties [3]. Table 2 also shows the systematic errors on Δm for ϕ_{+-} fixed.

Table 2. Systematic errors on the fitted values of ϕ_{+-} and $|\eta_{+-}|$ (for Δm fixed) and of Δm (for ϕ_{+-} fixed)

Source	ϕ_{+-}	$\lvert\eta_{+-}\rvert\times10^{3}$	$\Delta m\times10^{7}\hbar\mathrm{s}^{-1}$
Background level	$0.09°$	0.010	0.9
Background shape	$0.04°$	0.005	0.5
Changes in cuts	$0.16°$	0.008	3.0
Decay-time resolution	$0.06°$	0.010	0.2
Normalization procedure	$0.07°$	0.001	0.3
Absolute time scale	$0.03°$	0.001	0.1
Regeneration	$0.19°$	0.019	0.7
Total syst. error	$\mathbf{0.28°}$	**0.026**	**3.3**
$\sigma(\Delta m)$	$0.42°$	0.001	
$\sigma(\tau_S)$	$0.03°$	0.007	

7.3 Final results

Our final results for η_{+-}, with Δm and τ_S fixed at the world-average values from [3], are

$$|\eta_{+-}| = (2.264 \pm 0.023_{\mathrm{stat}} \pm 0.026_{\mathrm{syst}} \pm 0.007_{\tau_S}) \times 10^{-3} ,$$
$$\phi_{+-} = 43.19° \pm 0.53°_{\mathrm{stat}} \pm 0.28°_{\mathrm{syst}} \pm 0.42°_{\Delta m} .$$

These results have approximately the same errors as the averages of all previous experiments [3], enabling the precision on the world-average values to be improved by almost a factor of $\sqrt{2}$.

8 Summary and conclusions

Using a technique involving time-dependent decay-rate asymmetries between the decays of neutral kaons whose strangeness has been tagged at production, CPLEAR has measured both the magnitude and phase of the parameter η_{+-}, describing CP violation in the case of neutral kaons decaying to $\pi^+\pi^-$. Our results have a precision comparable to that of the current world-average values. Our value for ϕ_{+-} is in good agreement with the superweak phase [3]

$$\phi_{\mathrm{sw}} = \arctan[\frac{2\Delta m}{\Delta\Gamma}] = 43.50° \pm 0.08°,$$

where $\Delta\Gamma = \Gamma_S - \Gamma_L$, and is hence consistent with CPT invariance.

These results for η_{+-}, along with other CPLEAR results and the most recent world-average values for other neutral-kaon parameters, have recently been used, together with the constraints of unitarity, to determine $\mathrm{Im}(\delta)$ with significantly increased accuracy, and also to somewhat reduce the error on $\mathrm{Re}(\delta)$ [23]. These parameters have, in turn, been used to improve considerably the limits on the K^0-$\overline{\mathrm{K}}^0$ mass and decay-width differences [12].

By considering the variations of the fitted values of ϕ_{+-} and $|\eta_{+-}|$ with the gravitational potential, CPLEAR has also recently made stringent tests of the Equivalence Principle for particles and antiparticles [24].

Acknowledgements. We would like to thank the CERN LEAR staff for their support and co-operation, as well as the technical and engineering staff of our institutes. This work was supported by the following agencies: the French CNRS/Institut National de Physique Nucléaire et de Physique des Particules, the French Commissariat à l'Energie Atomique, the Greek General Secretariat of Research and Technology, the Netherlands Foundation for Fundamental Research on Matter (FOM), the Portuguese National Board for Science and Technology (JNICT), the Ministry of Science and Technology of the Republic of Slovenia, the Swedish Natural Science Research Council, the Swiss National Science Foundation, the UK Particle Physics and Astronomy Research Council (PPARC), and the US National Science Foundation.

References

1. E. Gabathuler and P. Pavlopoulos, Proc. of the Workshop on Physics at LEAR with Low Energy Cooled Antiprotons (Erice, 1982), eds. U. Gastaldi and R. Klapisch (Plenum, New York, 1984) p. 747
2. A. Apostolakis et al., CPLEAR Collaboration, Phys. Lett. B 458 (1999) 545

3. C. Caso et al., Particle Data Group, Eur. Phys. J. C 3 (1998) 1
4. R. Adler et al., CPLEAR Collaboration, Phys. Lett. B 369 (1996) 367
5. C. Geweniger et al., Phys. Lett. B 48 (1974) 487
6. W. Carithers et al., Phys. Rev. Lett. 34 ((1975) 1244
7. R. Carosi et al., NA31, Phys. Lett. B 237 (1990) 303
8. L.K. Gibbons et al., E731, Phys. Rev. Lett. 70 (1993) 1198
9. B. Schwingenheuer et al., E773, Phys. Rev. Lett. 74 (1995) 4376
10. J.H. Christenson et al., Phys. Rev. Lett. 43 (1979) 1212
11. R. Adler et al., CPLEAR Collaboration, Phys. Lett. B 363 (1995) 243 (these data are a subset of the total given in the present paper)
12. A. Angelopoulos et al., CPLEAR Collaboration, Phys. Lett. B 471 (1999) 332
13. R. Adler et al., CPLEAR Collaboration, Phys. Lett. B 363 (1995) 237
14. R. Adler et al., CPLEAR Collaboration, and J. Ellis, J.L. Lopez, N.E. Mavromatos, D.V. Nanopoulos, Phys. Lett. B 364 (1995) 239
15. F. Benatti, R. Floreanini, Phys. Lett. B 401 (1997) 337
16. H.-J. Gerber, Phys. Rev. Lett. 80 (1998) 2969
17. A. Angelopoulos et al., CPLEAR Collaboration, Phys. Lett. B 444 (1998) 52
18. R. Adler et al., CPLEAR Collaboration, Nucl. Instrum. Methods A 379 (1996) 76
19. P.H. Eberhard and F. Uchiyama, Nucl. Instrum. Methods A 350 (1994) 144
20. A. Angelopoulos et al., CPLEAR Collaboration, Phys.Lett. B 413 (1997) 422
21. A. Angelopoulos et al., CPLEAR Collaboration, Phys. Lett. B 444 (1998) 38
22. Determination of the position accuracy in CPLEAR, Internal Note, CPLEAR/DET/96-03, October 1996
23. A. Apostolakis et al., CPLEAR Collaboration, Phys. Lett. B 456 (1999) 297
24. A. Apostolakis et al., CPLEAR Collaboration, and J. Ellis, N.E. Mavromatos, D.V. Nanopoulos, Phys. Lett. B 452 (1999) 425